Pergamon

Int. J. Heat Mass Transfer. Vol. 40, No. 13, pp. 3039–3047, 1997

Printed in Great Britain
0017-9310/97 $17.00+0.00

PII: S0017-9310(96)00355-9

A model for convective mass transport in liquid phase epitaxial growth of semiconductors

S. DOST and Z. QIN
Department of Mechanical Engineering, University of Victoria, Victoria, B.C. V8W 3P6, Canada

and

M. KIMURA
Research Institute of Electronics, Shizuoka University, Hamamatsu 432, Japan

(*Received* 15 *April* 1996 *and in final form* 16 *October* 1996)

Abstract—A numerical simulation model for the convective mass transport occurring during the liquid phase epitaxial growth of GaInAs is presented. The mass transport and fluid flow equations in the liquid phase, mass transport equation in the solid phase and the relationships between concentrations and temperature obtained from the phase diagram constitute the governing equations. These equations together with appropriate interface and boundary conditions were solved numerically by the finite element method for a sandwich growth system. Numerical results show that the solutal convection plays an important role in this materials processing technique, enhances growth rate and influences compositional uniformity of the grown crystals. © 1997 Elsevier Science Ltd.

INTRODUCTION

Liquid phase epitaxy (LPE) is a solution growth technique for obtaining single crystal materials. In a typical LPE setup the furnace temperature is reduced gradually upon putting the liquid solution and a single crystal substrate in contact. The gradual reduction in temperature results in supersaturated solution in the vicinity of the solution–substrate interface, leading to the growth of high quality, single crystal layers. In LPE, the growth of ternary alloy materials is much more complex than the growth of binary compounds. The reason for this is that in LPE growth of ternary alloys the solid and liquid phases are close to equilibrium at their interface, thus the substrate (or grown layer) interacts with the liquid solution and hence actively participates in the formation of the current layer. The active interaction between the solid and liquid phases in LPE growth can only be modeled by complicated interface conditions which make numerical simulations extremely difficult. The numerical simulations that relied on a "starting solution" [1–3] is not general enough to simulate the complex growth processes of ternary alloys. In LPE crystal growth, convection in the liquid phase plays an important role [4–8]. An accurate simulation of the LPE growth process must include convection transport in the model.

We here present a numerical simulation model for the LPE growth process of GaInAs ternary alloy. The main objective of this study is to determine optimum growth conditions for better crystals by providing a better understanding for the role of natural convection in LPE growth. The mathematical model developed here accounts for diffusive and convective mass transport and fluid flow in the liquid, diffusive mass transport in the solid and phase equilibrium and mass conservation at the growing interface. The governing equations particularized for an LPE sandwich growth system are solved by the finite element technique. Numerical simulation results show that solutal convection plays an important role in this materials processing technique, enhances growth rates and influences compositional uniformity of the grown crystals.

GOVERNING EQUATIONS

For a III–III–V ternary alloy, i.e. an $A_xB_{1-x}C$ system (where A, B and C represent the components of the alloy), there are three compositional variables in the liquid phase, which must satisfy $x_A^l + x_B^l + x_C^l = 1$ where x_A^l, x_B^l and x_C^l are, respectively, the mole fractions of components A, B and C in the liquid. In this study A, B and C represent, respectively, gallium (Ga), indium (In) and arsenic (As). In the solid phase, only one compositional variable is needed to define solid composition distribution, since $x_A^s = 0.5x$, $x_B^s = 0.5(1-x)$ and $x_C^s = 0.5$ where x_A^s, x_B^s and x_C^s represent, respectively, the mole fractions of components A, B and C in the solid. In this study, we choose x_A^l and x_C^l as the independent compositional variables in the liquid and x_A^s, instead of x, as the compositional variable in the solid. All these variables are functions of time and space.

NOMENCLATURE

A, B, C components of a III–III–V ternary alloy
D_A^l diffusion coeffient of element A in the liquid
D_C^l diffusion coefficient of element C in the liquid
D_A^S diffusion coefficient of element A in the solid
d_{AC} lattice parameter of compound AC
d_{BC} lattice parameter of compound BC
d_{AC-BC} lattice parameter of alloy
f growth rate
Gr Grashof number
g graviational constant
L height of the liquid solution
N_{Av} Avogadro number
p pressure
p' dimensionless pressure
R gas constant
Sc Schmidt number
T growth temperature
T_F melting point
t time
u, v velocity components
u', v' dimensionless velocity components
X, Y coordinates
x solid composition
x_A^l, x_B^l, x_C^l mole fractions of elements A, B and C in the liquid
x_A^S, x_B^S, x_C^S mole fractions of elements A, B and C in the solid
x_{A0}^l, x_{C0}^l initial mole fractions of elements A and C in the liquid.

Greek symbols
ΔS^F entropy of fusion
β_A, β_C solutal expansion coefficients related to elements A and C
γ^l, γ^S activity coefficients in the liquid and solid phases
γ^{sl} activity coefficient in the stoichiometric liquid
ξ, η dimensionless coordinates
λ dimensionless growth rate
ν kinematic viscosity
τ dimensionless time
ρ_0 mass density of the liquid
ω^l more density of the liquid
ω^S more density of the solid.

In LPE, growth is often realized through programmed gradual temperature changes. Since the process is very slow and also the solution is a good heat conductor, temperature distribution is approximately uniform throughout the system, but its value changes with time. These temperature changes do not affect concentration distribution and fluid flow significantly, they mainly alter the phase relations at the crystal–liquid interface. Because they display equilibria, they can be viewed as external driving forces that act simultaneously with internal forces due to constitutional equilibria, i.e. the system initial compositions. In general, macroscopic growth of an epitaxial layer is affected by mass and heat transfer as well as fluid flow. Since the system temperature is decreased very slowly during growth, in simulations the growth process is assumed to be isothermal. The heat transfer balance includes, in general, the contribution of latent heat at the interface. However, since the velocity of growth interface is very small in LPE, the contribution of latent heat to the energy balance at the interface is not significant and is, therefore, neglected. Furthermore, the solution is assumed to be an incompressible, Newtonian fluid, and the well-known Boussinesq approximation holds (i.e. the density of the solution is constant in all equations except in the body force in the momentum equations). The solid phase is assumed to be rigid but the diffusion mass transport is allowed. The process and the system are assumed to be nominally two-dimensional.

Under the above assumptions, the system of equations governing the process consists of only the unsteady, two-dimensional, incompressible fluid flow and mass transport equations (these equations can also be obtained as a special case from the basic equations given for liquid phase electroepitaxial growth of a general ternary system in ref. [9], by neglecting contributions from the electric field). The energy balance is satisfied identically. The fluid flow equations take the following explicit forms in Cartesian coordinates.

Incompressibility

$$\frac{\partial u}{\partial X} + \frac{\partial v}{\partial Y} = 0. \tag{1}$$

Momentum

$$\frac{\partial u}{\partial t} + u\frac{\partial u}{\partial X} + v\frac{\partial u}{\partial Y} = -\frac{1}{\rho_0}\frac{\partial p}{\partial X} + \nu\left(2\frac{\partial^2 u}{\partial X^2} + \frac{\partial^2 u}{\partial Y^2} + \frac{\partial^2 v}{\partial X\,\partial Y}\right) \tag{2}$$

$$\frac{\partial v}{\partial t}+u\frac{\partial v}{\partial X}+v\frac{\partial v}{\partial Y}=-\frac{1}{\rho_0}\frac{\partial p}{\partial Y}+\nu\left(\frac{\partial^2 v}{\partial X^2}+2\frac{\partial^2 v}{\partial Y^2}+\frac{\partial^2 u}{\partial X\,\partial Y}\right)+g[\beta_A(x_A^l-x_{A0}^l)+\beta_C(x_C^l-x_{C0}^l)] \quad (3)$$

where u and v are the velocity components in the X and Y directions, respectively, t is time, p is pressure, ρ_0 is the density of the solution, ν is the kinematic viscosity, g is the gravitational constant, β_A and β_C are the solutal expansion coefficients related, respectively, to components A and C in the solution, and x_{A0}^l and x_{C0}^l are the initial mole fractions of components A and C in the solution, respectively.

A detailed derivation of mass transport equations is given in refs. [9, 10]. The principle of conservation of mass for components A and C in the liquid phase and for A in the solid phase yields the following mass transport equations:

in the liquid

$$\frac{\partial x_A^l}{\partial t}+u\frac{\partial x_A^l}{\partial X}+v\frac{\partial x_A^l}{\partial Y}=D_A^l\nabla^2 x_A^l$$

$$\frac{\partial x_C^l}{\partial t}+u\frac{\partial x_C^l}{\partial X}+v\frac{\partial x_C^l}{\partial Y}=D_C^l\nabla^2 x_C^l \quad (4)$$

in the solid

$$\frac{\partial x_A^s}{\partial t}=D_A^s\nabla^2 x_A^s+\frac{D_A^s}{\omega^s}\left(\frac{\partial\omega^s}{\partial X}\frac{\partial x_A^s}{\partial X}+\frac{\partial\omega^s}{\partial Y}\frac{\partial x_A^s}{\partial Y}\right) \quad (5)$$

where D_A^l, D_C^l and D_A^s are, respectively, the diffusivities of components A and C in the liquid phase and that of component A in the solid phase, ω^s is the total mole density of the solid, and $\nabla^2\equiv\partial^2/\partial X^2+\partial^2/\partial Y^2$. In equation (4), the total mole density in the liquid is assumed to be constant since it is mostly determined by the solvent. For most III–V alloys, the lattice parameters change notably from AC to BC leading to density variation. ω^s can be related to the solid composition, x, by [11]

$$\omega^s=\frac{8}{N_{Av}[xd_{AC}+(1-x)d_{BC}]^3} \quad (6)$$

where N_{Av} is the Avogadro number, d_{AC} and d_{BC} are the lattice parameters of components AC and BC, respectively, and we have assumed that the lattice parameter of an alloy, $d_{AC\text{-}BC}$, changes linearly from d_{AC} to d_{BC}.

For computational convenience, we choose the following dimensionless parameters

$$\xi=\frac{X}{L}\quad \eta=\frac{Y}{L}\quad \tau=\frac{tv}{L^2}\quad p'=\frac{pL^2}{\rho_0\nu^2}$$

$$u'=\frac{uL}{\nu}\quad v'=\frac{vL}{\nu}\quad Sc^A=\frac{\nu}{D_A^l}\quad Sc^C=\frac{\nu}{D_C^l}$$

$$Sc^S=\frac{\nu}{D_A^s}\quad Gr^A=\frac{g\beta_A L^3 x_{A0}^l}{\nu^2}\quad Gr^C=\frac{g\beta_C L^3 x_{C0}^l}{\nu^2} \quad (7)$$

where L is the height of the liquid solution. Then the governing equations take the following dimensionless forms:

in the liquid

$$\frac{\partial u'}{\partial\xi}+\frac{\partial v'}{\partial\eta}=0 \quad (8)$$

$$\frac{\partial u'}{\partial\tau}+u'\frac{\partial u'}{\partial\xi}+v'\frac{\partial u'}{\partial\eta}=-\frac{\partial p'}{\partial\xi}+2\frac{\partial^2 u'}{\partial\xi^2}+\frac{\partial^2 u'}{\partial\eta^2}+\frac{\partial^2 v'}{\partial\xi\,\partial\eta} \quad (9)$$

$$\frac{\partial v'}{\partial\tau}+u'\frac{\partial v'}{\partial\xi}+v'\frac{\partial v'}{\partial\eta}=-\frac{\partial p'}{\partial\eta}+\frac{\partial^2 v'}{\partial\xi^2}+2\frac{\partial^2 v'}{\partial\eta^2}+\frac{\partial^2 u'}{\partial\xi\,\partial\eta}+Gr^A\left(\frac{x_A^l}{x_{A0}^l}-1\right)+Gr^C\left(\frac{x_C^l}{x_{C0}^l}-1\right) \quad (10)$$

$$\frac{\partial x_A^l}{\partial\tau}+u'\frac{\partial x_A^l}{\partial\xi}+v'\frac{\partial x_A^l}{\partial\eta}=\frac{1}{Sc^A}\left(\frac{\partial^2 x_A^l}{\partial\xi^2}+\frac{\partial^2 x_A^l}{\partial\eta^2}\right) \quad (11)$$

$$\frac{\partial x_C^l}{\partial\tau}+u'\frac{\partial x_C^l}{\partial\xi}+v'\frac{\partial x_C^l}{\partial\eta}=\frac{1}{Sc^C}\left(\frac{\partial^2 x_C^l}{\partial\xi^2}+\frac{\partial^2 x_C^l}{\partial\eta^2}\right) \quad (12)$$

in the solid

$$\frac{\partial x_A^s}{\partial\tau}=\frac{1}{Sc^S}\left(\frac{\partial^2 x_A^s}{\partial\xi^2}+\frac{\partial^2 x_A^s}{\partial\eta^2}\right)+\frac{1}{Sc^S\omega^s}\left(\frac{\partial\omega^s}{\partial\xi}\frac{\partial x_A^s}{\partial\xi}+\frac{\partial\omega^s}{\partial\eta}\frac{\partial x_A^s}{\partial\eta}\right). \quad (13)$$

The mass balance between the transported and incorporated solute species gives the mass balance interface conditions [8]. These conditions in their dimensionless forms are obtained as follows

$$\Delta_\omega\lambda(x_A^{s0}-x_A^{l0})=\left.\frac{\partial x_A^l}{\partial\eta}\right|_0-\Delta_\omega\Delta_s\left.\frac{\partial x_A^s}{\partial\eta}\right|_0$$

$$\Delta_\omega\lambda(0.5-x_C^{l0})=\Delta_l\left.\frac{\partial x_C^l}{\partial\eta}\right|_0 \quad (14)$$

where we have used $x_C^s=0.5$ and x_A^{s0}, x_A^{l0} and x_C^{l0} are the mole fractions at the interface, and

$$\Delta_\omega=\frac{\omega^s}{\omega^l}\quad \Delta_s=\frac{D_A^s}{D_A^l}\quad \Delta_l=\frac{D_C^l}{D_A^l}\quad \lambda=\frac{fL}{D_A^l} \quad (15)$$

where f is the growth rate.

Needed two more equations are obtained from the condition that the compositions of the phases must also satisfy the phase diagram at the interface. The liquid phase is assumed to be in equilibrium with the desired composition of the epitaxial layer to be grown. In general, the initial substrate has a different com-

position from the new layer. The initial condition is determined by phase diagram based on the growth temperature and the solid composition with which the liquid should be in equilibrium. The phase diagram for a ternary III–V system $A_xB_{1-x}C$ can be described by the following equations [10]:

$$\gamma^s_{AC}x = \frac{4\gamma^l_A\gamma^l_C x^l_A x^l_C}{\gamma^{sl(AC)}_A\gamma^{sl(AC)}_C}\exp\left[\frac{\Delta S^F_{AC}(T^F_{AC}-T)}{RT}\right] \quad (16)$$

$$\gamma^s_{BC}(1-x) = \frac{4\gamma^l_B\gamma^l_C x^l_B x^l_C}{\gamma^{sl(BC)}_B\gamma^{sl(BC)}_C}\exp\left[\frac{\Delta S^F_{BC}(T^F_{BC}-T)}{RT}\right] \quad (17)$$

where γ^l and γ^s are the activity coefficients in the liquid and solid phase, respectively, γ^{sl} are the activity coefficients in the stoichiometric liquid, ΔS^F_{AC} and ΔS^F_{BC} are the entropies of fusion, T^F_{AC} and T^F_{BC} are the melting points, R is the gas constant, and T is the growth temperature. Here the solid solution of composition $A_xB_{1-x}C$ is treated as a mixture of the binary solids AC and BC, separate equilibrium conditions are written for AC in the solid phase, A and C in the ternary liquid and for BC in the solid phase and B and C in the liquid phase. Since the activity coefficients are related to the compositions and temperature, the phase diagram equations are nonlinear. Newton–Raphson method is used to solve for compositions of A and C in the solution. In the solid phase, the initial condition is the substrate composition.

It is important to note that, for ternary alloys, solid composition is not simply determined by phase diagram, but also by the ratio of transport rates of solutes. This makes numerical simulations for ternary systems much more complicated than for binary systems in which equilibrium deposition may be assumed. Unlike the pure diffusion case, the interface concentrations and the growth rate vary along the interface even for the constant temperature distribution because the concentration gradients vary along the interface due to the effect of natural convection. Therefore, the interface conditions must be enforced at all nodes along the interface.

NUMERICAL SOLUTION METHOD

The governing equations given in the preceding section are difficult to solve because of the complex interface conditions and the nonlinear coupling of the solid and liquid phase equations. The finite element method based on the penalty function formulation is used in this study. The advantage of the penalty function formulation is that the additional flow variable pressure is eliminated and so is the need for solving the incompressibility condition, which avoids the well-known difficulties of the mixed velocity/pressure formulation in incompressible flows and makes it easy to implement the complicated problem [13]. The Galerkin method and 4-node quadrilateral elements are used to discretize the governing equations. To insure that the element possesses the mean incompressibility property, the reduced integration is used [14]. All integrals are evaluated using a 2×2 Gaussian quadrature over each element, except for the penalized terms which are evaluated using 1-point Gauss rule. The resulting set of first-order simultaneous ordinary differential equations with time derivatives are further discretized by fully implicit time-marching algorithm based on the finite difference method. The nonlinear algebraic equations resulting from the implicit approximation at each time step are solved by the Newton–Raphson iteration.

Since the physical parameters are very different in the solid and liquid phases, a separated solution procedure is applied to avoid numerical difficulties due to large differences in the matrix elements, i.e. the governing equations are solved separately for the solid and liquid phases, by using different mesh size and different time scale in the two phases. The two phases are actually coupled by the growth rate and the interface condition. An iteration procedure is then applied to obtain convergent solutions in the two phases and at the interface for each time step. Upon the convergence of the solution, growth thickness is readily computed by integrating the growth rate. Then the finite element mesh moves to track the moving interface.

The transient solution of the governing equations for LPE growth of ternary alloys is very time consuming. A combined full and modified Newton–Raphson iteration scheme is used, namely, the full Newton–Raphson method is used in the first iteration for each time step and the modified Newton–Raphson method is used during the subsequent iterations until the solutions for the bulk phases and the interfaces are converged. This solution scheme significantly reduces computation time since the modified Newton–Raphson method requires fewer reformations and factorizations of the tangent stiffness matrix and still provides a reasonable convergence speed.

The overall computational procedure consists of the following steps:

(1) Set initial growth configuration and finite element mesh.
(2) Calculate initial composition of the solution using phase diagram.
(3) Guess initial interface condition based on the thermodynamic mode [8].
(4) Start time integration.
(5) Perform Newton–Raphson iterations for finite element solutions of the bulk phases.
(6) Calculate interface concentrations and growth rate.
(7) Check convergence of the solutions for the bulk phases and the interfaces.
(8) Modify interface conditions and return to step 5 if convergence is not achieved.
(9) Update finite element mesh and forward to next time step if convergence is achieved.

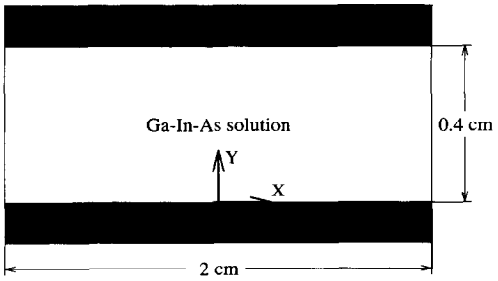

Fig. 1. Schematic view of LPE growth configuration.

RESULTS AND DISCUSSION

The numerical simulations are carried out for a sandwich system consisting of a substrate solution–substrate arrangement for growth of $Ga_{0.1}In_{0.9}As$ from In-rich solution. The upper and lower substrates are InAs and GaAs, respectively. A schematic view of the growth cell is shown in Fig. 1. The initial temperature of the growth cycle is 700°C. The growth is achieved by reducing the temperature gradually at the rate of 0.25°C min^{-1}. The initial solution composition determined by phase diagram is $x^l_{Ga} = 0.0194$, $x^l_{In} = 0.8732$ and $x^l_{As} = 0.1074$. The physical parameters used in simulations are listed in Table 1. Because few measurements are available to correlate accurately the physical parameters needed for numerical modelling, we have to rely on approximate expressions to evaluate those parameters for which experimental data are not available. The solutal diffusivities are estimated using the expression in ref. [16] for self diffusion of indium liquid. The solid diffusivity is estimated following [1]. The solutal expansion coefficients are estimated using the expression given in ref. [17].

In the growth process, the deposition of the lower density solutes on the substrates increases the density of the solution in the vicinity of the substrates. Therefore, unstable stratification develops in the upper region, leading to buoyancy-induced convective flow which in turn affects mass transport in the solution. The evolution of the velocity field is shown in Fig. 2. The flow cells are mainly located in the vicinity of the upper substrate and move along the interface. The magnitude of the velocity generated by natural convection is about 3×10^{-2} cm s^{-1}. The convective flow in the solution results in higher concentration gradients near the upper substrate. Figure 3 shows the isoconcentrations of Ga in the solution. The higher concentration gradients at the upper substrate interface result in faster growth rate in the upper substrate than that in the lower substrate. The concentration patterns for As are similar since the same diffusion coefficient is used for the solutes in the simulations. Due to higher solubility, the mass flux of As is larger than that of Ga. The ratio of the mass fluxes affects growth rate and solid composition.

In addition to enhancing mass transport rate, convection also influences composition uniformity of the grown crystals. Figure 4 shows a comparison between the composition profiles computed by diffusion and convection models for the conventional LPE with a constant cooling rate. As expected, the composition profiles of the grown crystals are significantly graded due to the continuous cooling and the solute depletion as growth proceeds. Since convection brings extra solutes to the vicinity of the growing substrate and leads to effective mixture of the solution, better composition uniformity is predicted by the convection model.

The computed growth rates for the upper and lower substrates, averaged along the substrate surfaces, are shown in Fig. 5. At the beginning of the growth process, growth rates increase rapidly and remain identical for both substrates, indicating that growth is controlled by diffusion. After the onset of natural convection, bifurcation of growth rate curves for the upper and lower substrates takes place and the growth rate of the upper substrate increases continuously. After the development of convective flow, growth rate varies around an almost constant average value with small amplitudes and nearly steady-state growth takes place. The oscillatory patterns of the average growth rate curves are due to the non-uniform growth rates along the substrates which are attributed to the unsteady convective flow. At the end of the growth period, growth is stopped and temperature is held constant until the dissolution process begins. During this period, as can be seen from the curves, growth rates decrease first rapidly and then stop when solute elements are depleted completely in the solution.

Table 1. Physical parameters

Parameters	Symbols	values
Solution viscosity [15]	ν	$10^{-3}cm^2s^{-1}$
Solutal diffusivity of Ga	D^l_A	$8.2 \times 10^{-5}cm^2s^{-1}$
Solutal diffusivity of As	D^l_C	$8.2 \times 10^{-5}cm^2s^{-1}$
Solid diffusivity	D^S_A	$1 \times 10^{-12}cm^2s^{-1}$
Solutal expansion coefficient	β_A	-0.12
Solutal expansion coefficient	β_C	-0.19
Mole density of the solution [16]	ω^l	0.0596 mol cm^{-3}
Lattice parameter of GaAs [11]	d_{AC}	5.6533
Lattice parameter of InAs [11]	d_{BC}	6.0584
Solution height	L	0.4 cm

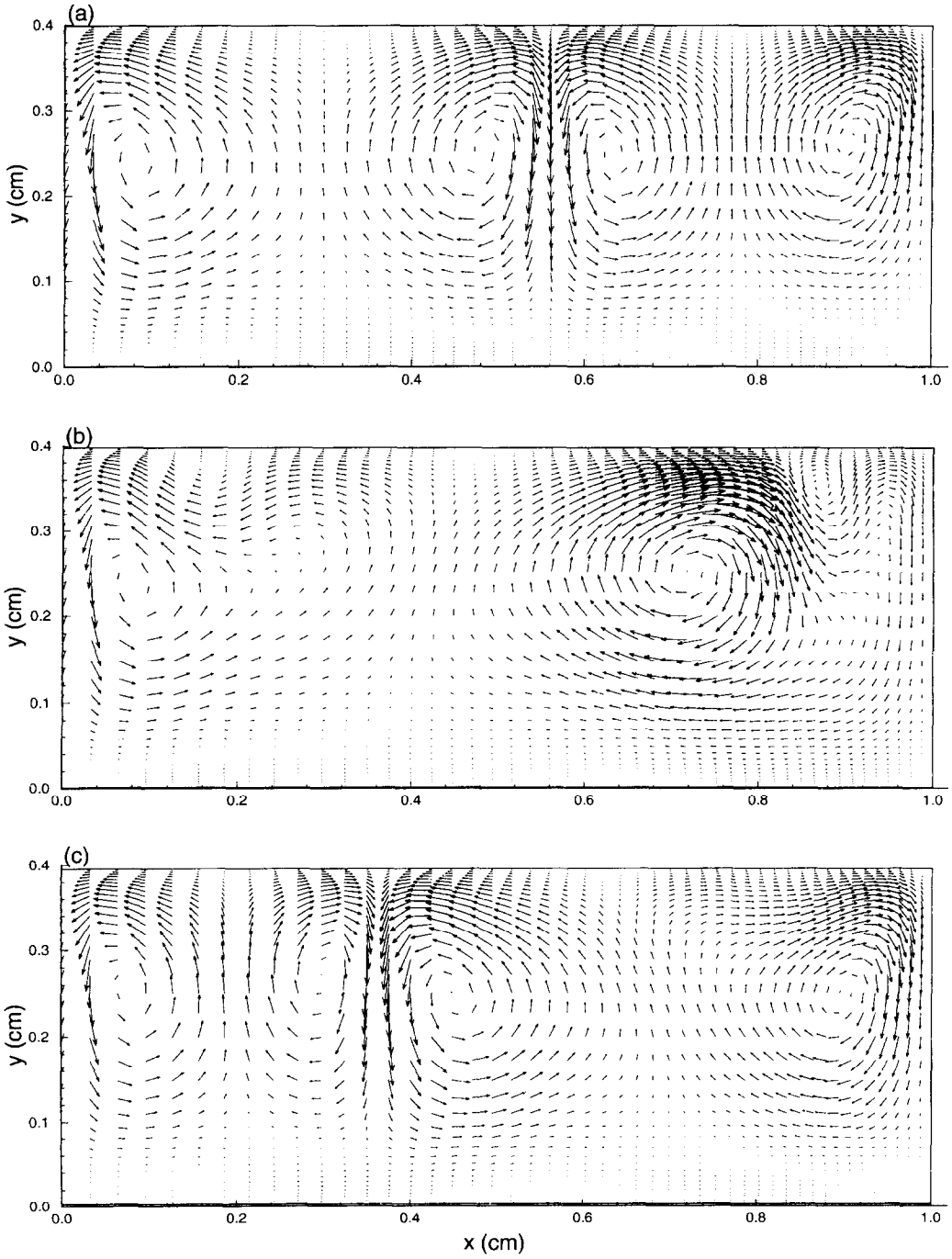

Fig. 2. Evolution of velocity fields: (a) $t = 10$ min; (b) $t = 20$ min; (c) $t = 30$ min.

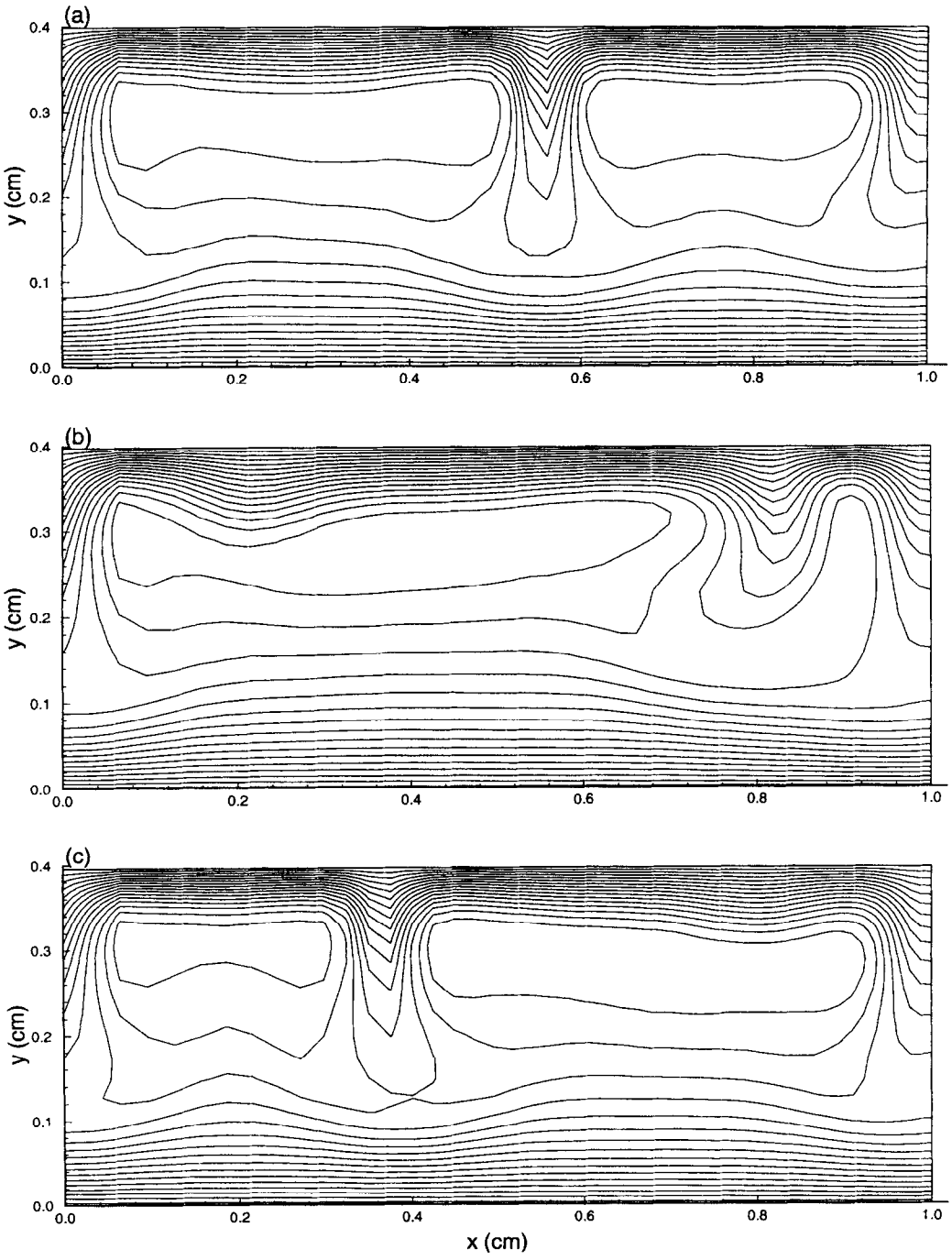

Fig. 3. Evolution of concentration patterns: (a) $t = 10$ min; (b) $t = 20$ min; (c) $t = 30$ min.

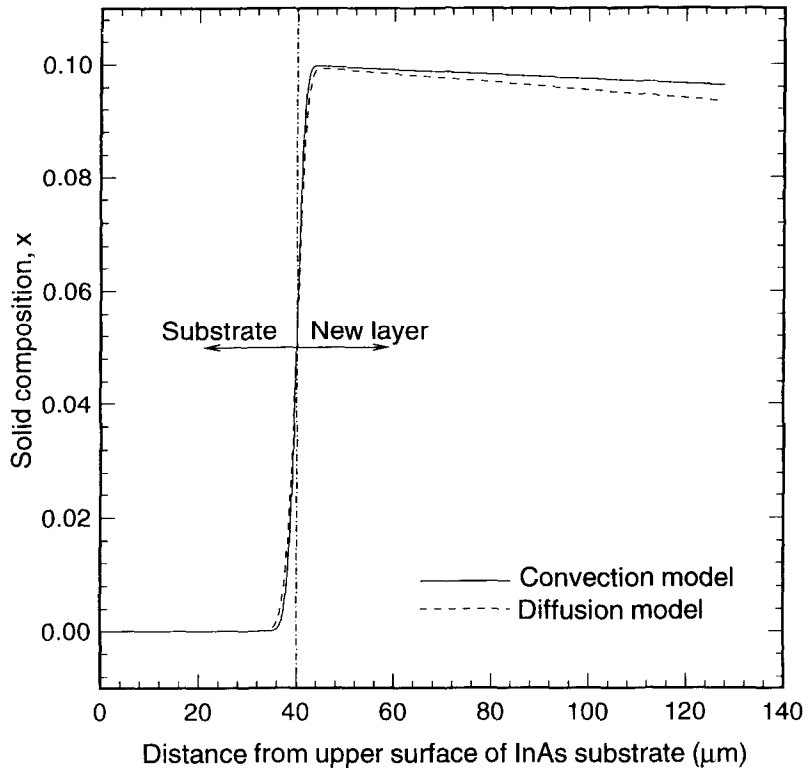

Fig. 4. Comparison of computed profiles of solid composition by convection and diffusion models

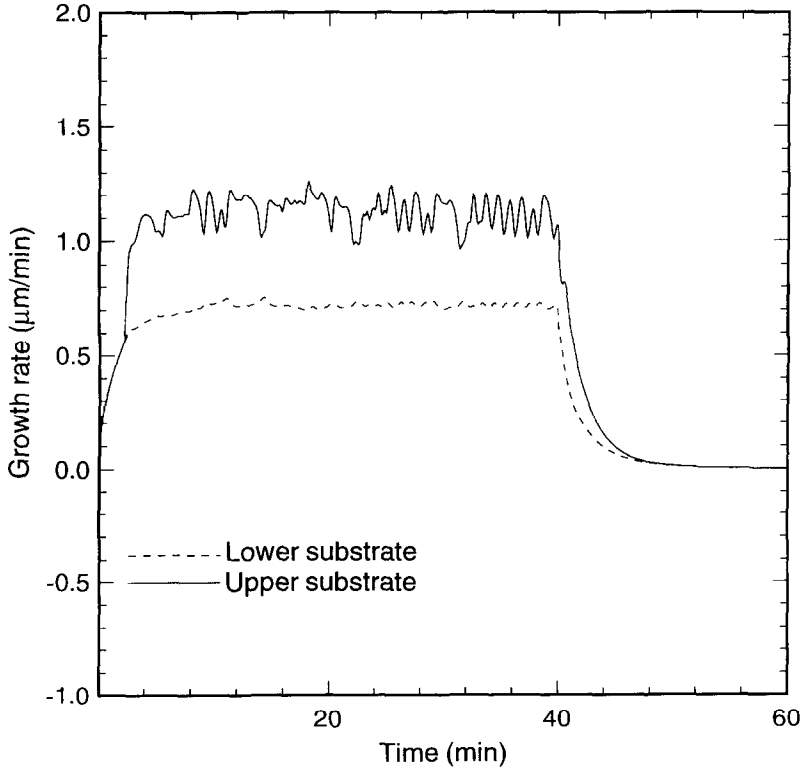

Fig. 5. Time history of average growth rates for upper and lower substrates.

The simulation results clearly show that the upper substrate grows more than the lower one. The thicknesses of grown layers obtained from the simulation are about 46 μm for the upper substrate and 28 μm for the lower substrate after 40 min of growth. These values are very close to those obtained from experiments. The measured difference in grown thicknesses of the upper and lower substrates is about 14 μm.

CONCLUSION

In this article a numerical simulation study for the role of solutal convection on the mass transport occurring during LPE growth of ternary III–V alloys has been presented. The governing equations of the liquid and solid phases, together with interface and phase equilibrium equations were solved using the finite element method and Newton–Raphson iteration. The simulation results presented in this article have demonstrated that natural convection plays a crucial role in liquid phase epitaxial growth of ternary alloys. Natural convection influences growth rates and composition uniformity. Numerical results agree with experiments.

Acknowledgment—The work presented here was supported by the Research Institute of Electronics, Shizuoka University, Hamamatsu, Japan and the Natural Sciences and Engineering Research Council of Canada (NSERC).

REFERENCES

1. Small, M. B. and Ghez, R., Growth and dissolution kinetics of III–V heterostructures formed by LPE. *Journal of Applied Physics*, 1979, **50,** 5322.
2. Small, M. B. and Ghez, R., Growth and dissolution kinetics of III–V heterostructures formed by LPE. II. *Journal of Applied Physics*, 1980, **51,** 1589.
3. Ghez, R. and Small, M. B., Growth and dissolution kinetics of ternary III–V heterostructures formed by LPE. III. Effects of temperature programming. *Journal of Applied Physics*, 1982, **53,** 4907.
4. Sukegawa, T., Kimura, M. and Tanaka, A., Gravity effect on dissolution and growth of silicon in the In–Si system. *Journal of Crystal Growth*, 1988, **92,** 46.
5. Erbay, S., Erbay, H. A., Djilali, N. and Dost, S., Investigation of solutal convection during the dissolution of silicon in a sandwich system. *International Journal of Heat and Mass Transfer*, 1993, **36,** 3017.
6. Kimura, M., Djilali, N. and Dost, S., Convective transport and interface kinetics in liquid phase epitaxy. *Journal of Crystal Growth*, 1994, **143,** 334.
7. Dost, S. and Erbay, H. A., A continuum model for electroepitaxy. *International Journal of Engineering Science*, 1995, **33,** 1385.
8. Kimura, M., Qin, Z. and Dost, S., A solid–liquid diffusion model for ternary semiconductor alloys. *Journal of Crystal Growth*, 1996, **158,** 231–240.
9. Dost, S. and Qin, Z., A model for liquid phase electroepitaxial growth of ternary alloy semiconductors. *International Journal of Applied Electromagnetics and Mechanics*, 1996, **7,** 109.
10. Dost, S., Recent developments in liquid phase electroepitaxy: a continuum approach. *Applied Mechanics Reviews*, 1996, **49,** 477.
11. Panish, M. B. and Ilegems, M., Phase equilibria in ternary III–V systems. *Progress in Solid State Chemistry*, 1972, **7,** 39.
12. Casey, Jr. H. C. and Panish, M. B., *Heterostructure Lasers*. Academic Press, New York, 1978.
13. Qin, Z., Dost, S., Djilali, N. and Tabarrok, B., A model for liquid phase electroepitaxy under an external magnetic field—II. Application. *Journal of Crystal Growth*, 1995, **153,** 131.
14. Hughes, T. J. R., Liu, W. K. and Brooks, A., Finite element analysis of incompressible viscous flows by the penalty function formulation. *Journal of Computational Physics*, 1979, **30,** 1.
15. Bryskiewicz, T. and Laferriere, A., Growth of alloy substrate by liquid phase electroepitaxy: theoretical considerations. *Journal of Crystal Growth*, 1993, **129,** 429.
16. Smithells, C. J. and Brandes, E. A., *Metals Reference Book*. Butterworths, London, 1976.
17. Long, S. I., Ballantyne, J. M. and Easrman, L. F., Steady-state LPE growth of GaAs. *Journal of Crystal Growth*, 1974, **26,** 13.